CCS Chemistry

RESEARCH ARTICLE

Received: Nov. 1, 2023 | Accepted: Nov. 21, 2023 | Published: Dec. 27, 2023

An Integrated Carbon Dioxide Capture and Methanation Process

Xiaochen Zhang[1†], Mengzhu Li[1,2†], Xingwu Liu[1,3†], Ang Li[4†], Yuchen Deng[1], Mi Peng[1], Yu Zhang[3], Charlotte Vogt[5], Matteo Monai[5], Junxian Gao[1], Xuetao Qin[1], Yao Xu[1], Qiaolin Yu[1], Meng Wang[1], Guofu Wang[6], Zheng Jiang[7], Xiaodong Han[4], Casper Brady[8], Wei-Xue Li[9,10], Wu Zhou[11]*, Jin-Xun Liu[8,10]*, Bingjun Xu[1,8]*, Bert M. Weckhuysen[5]* & Ding Ma[1]*

[1]Beijing National Laboratory for Molecular Sciences, College of Chemistry and Molecular Engineering, Peking University, Beijing 100871, [2]China Academy of Aerospace Science and Innovation, Beijing 100088, [3]National Energy Center for Coal to Liquids, Synfuels China Co., Ltd., Beijing 101400, [4]Beijing Key Laboratory of Microstructure and Property of Advanced Materials, Beijing University of Technology, Beijing, [5]Inorganic Chemistry and Catalysis group, Institute for Sustainable and Circular Chemistry and Debye Institute for Nanomaterials Science, Faculty of Science, Utrecht University, 3584 CG Utrecht, [6]State Key Laboratory of Coal Conversion, Institute of Coal Chemistry, Chinese Academy of Sciences, Taiyuan 030001, [7]Shanghai Synchrotron Radiation Facility, Zhangjiang Lad, Shanghai Advanced Research Institute, Chinese Academy of Sciences, Shanghai 201210, [8]Center for Catalytic Science and Technology, University of Delaware, Newark, Delaware 19716, [9]Key Laboratory of Precision and Intelligent Chemistry, School of Chemistry and Materials Science, University of Science and Technology of China, Hefei, Anhui 230026, [10]Hefei National Laboratory, University of Science and Technology of China, Hefei 230088, [11]School of Physical Sciences, CAS Key Laboratory of Vacuum Physics, University of Chinese Academy of Sciences, Beijing 100049

**Corresponding authors: dma@pku.edu.cn; B.M.Weckhuysen@uu.nl; bxu@pku.edu.cn; jxliu86@ustc.edu.cn; wuzhou@ucas.ac.cn; †X. Zhang, M. Li, X. Liu, and A. Li contributed equally to this work.*

Cite this: *CCS Chem.* **2023**, Just Published. DOI: 10.31635/ccschem.023.202303594

Reducing the ever-growing level of CO_2 in the atmosphere is critical for the sustainable development of human society in the context of global warming. Integration of the capture and upgrading of CO_2 is, therefore, highly desirable since each process step is costly, both energetically and economically. Here, we report a CO_2 direct air capture (DAC) and fixation process that produces methane. Low concentrations of CO_2 (~400 ppm) in the air are captured by an aqueous solution of sodium hydroxide to form carbonate. The carbonate is subsequently hydrogenated to methane, which is easily separated from the reaction system, catalyzed by TiO_2-supported Ru in the aqueous phase with a selectivity of 99.9% among gas-phase products. The concurrent regenerated hydroxide, in turn, increases the alkalinity of the aqueous solution for further CO_2 capture, thereby enabling this one-of-its-kind continuous CO_2 capture and methanation process. Engineering simulations demonstrate the energy feasibility of this CO_2 DAC and methanation process, highlighting its promise for potential large-scale applications.

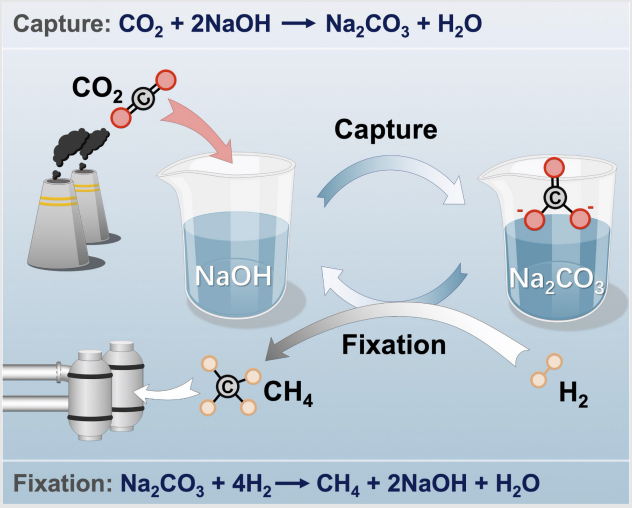

Keywords: CO_2 capture and methanation process, sodium hydroxide, carbonate, Ru/TiO_2, catalytic mechanism, CO_2 activation and hydrogenation

Citation: *CCS Chem.* **2023**, Just Published. DOI: 10.31635/ccschem.023.202303594
Link to VoR: https://doi.org/10.31635/ccschem.023.202303594

Introduction

Accelerating the transition of the current fossil carbon-dependent economy to a renewable energy-based one is increasingly urgent as the anthropogenic climate change exacts a rapidly growing economic and humanitarian toll across the globe.[1,2] Projections recent reports by the Intergovernmental Panel on Climate Change make it clear that not only should CO_2 emissions be drastically cut, but also that a significant fraction of CO_2 in the atmosphere must be scrubbed to evade the most dire consequences of climate change.[3,4] Capture of diluted CO_2 in airtight living structures like space vehicles and transforming it on-site into fuels is also crucial for manned space explorations. A key challenge facing our society is the lack of economically viable technologies to capture and upgrade CO_2 from distributed point sources and the atmosphere.[5] Considerable effort has been devoted to tackling specific aspects of this challenge, such as CO_2 capture and fixation. For example, multiple direct air capture (DAC) strategies for CO_2 are being explored, including temperature/humidity swing adsorption with liquid amines,[6] processes similar to the Kraft Caustic Recovery Cycle (KCRC),[7] and a thermochemical cycle.[8] However, it remains challenging to employ these technologies in the near future due to their high cost and/or low technological maturity.[9,10] On the CO_2 upgrading front, progress has been made in both the electrocatalytic and thermocatalytic routes;[11–17] however, they typically require a high-purity CO_2 stream.[18] In this context, integrated CO_2 capture and fixation processes are highly desirable for their potential to be deployed both at point sources of CO_2 emissions, for example, thermal power plants and industrial sites, and in a distributed fashion for DAC.[19–22] To make such processes economically viable, a key consideration is the potential for downstream process intensification,[19] for example, by easing the separation of products from the reaction medium. Recent work reported an integrated CO_2 capture and fixation process by using an alkaline medium to capture CO_2, followed by its conversion to methanol.[21] Although methanol is a valuable chemical, its energetically costly separation from the reaction mixture limits its economic viability. Similarly, selectivity control in the thermo/electrocatalytic conversion of CO_2 to a single product is challenging,[23] and the separation of multiple gaseous and liquid products into valuable pure compounds is also costly. Therefore, given the demonstrated absorption efficacy of CO_2, especially at low concentrations, by alkaline liquid media, production of a single gaseous product from the captured CO_2 with high selectivity to enable facile separation would be highly advantageous.

In this work, we report an integrated CO_2 capture and methanation (CC&M) process. Dilute CO_2 is captured by an alkaline solution, and the produced carbonate is selectively hydrogenated on a Ru-based catalyst to methane with a selectivity of 99.9% among gas-phase products, which also regenerates the base and completes the cycle (Figure 1a). The net effect of this circular process is to capture CO_2 in a dilute gas feed, such as air or industrial emissions, and produce a pure/concentrated methane stream. Provided that the hydrogen needed in this process is supplied from renewable sources, our preliminary technoeconomic analysis suggests that the proposed CC&M process can enable a renewable circular economy. With low-cost renewable hydrogen increasingly available, the proposed CC&M process would be both environmentally beneficial and economically viable.

Experimental Methods

The experimental details are available in the Supporting Information, including the synthesis of catalysts, evaluation of catalytic performance, CO_2 air capture, structural characterization, process simulation methods, and density functional theory (DFT) calculations.

Results and Discussion

Alkaline aqueous solutions are known to be able to effectively capture dilute CO_2, and can be used in the DAC of CO_2.[7] To confirm that low-level (400 ppm) CO_2 in the air can be effectively absorbed by NaOH solution, we have first performed a simplified laboratory-scale CO_2 capture experiment by bubbling the ambient air into the alkaline solution. More than 90% of the CO_2 in the atmosphere (~400 ppm) was absorbed by passing air through an alkaline solution of sodium hydroxide and sodium carbonate (pH = 13.5, similar to that after the hydrogenation of carbonate, see below), at room temperature (Figure 1b). CO_2 concentration in the exhaust did not rise appreciably until all OH^- was converted to CO_3^{2-} (pH ~ 11.7). Afterward, the CO_2 concentration gradually recovered to ~400 ppm as CO_3^{2-} was further converted to HCO_3^-. No appreciable CO_2 in the feed was absorbed when the solution pH reached 10.8, which roughly corresponded to the complete conversion of CO_3^{2-} to HCO_3^- according to well-established aqueous phase equilibria.[24] Therefore, we can expect effective DAC (>90% CO_2 capture) given sufficient gas/liquid contact (which can be easily achieved in industrial processes) and that the pH of the solution can be maintained above ~11.7, which corresponds to capturing 90% of CO_2 in ~1.2×10^4 L of air per liter of solution after carbonate hydrogenation (pH = 13.5). The viability of the proposed DAC strategy on an industrial scale is confirmed in the process simulations based on a CC&M plant (see below).

Since CO_3^{2-} becomes dominant in the aqueous phase after the CO_2 DAC process, it is pivotal to develop a new

Citation: *CCS Chem.* **2023**, Just Published. DOI: 10.31635/ccschem.023.202303594
Link to VoR: https://doi.org/10.31635/ccschem.023.202303594

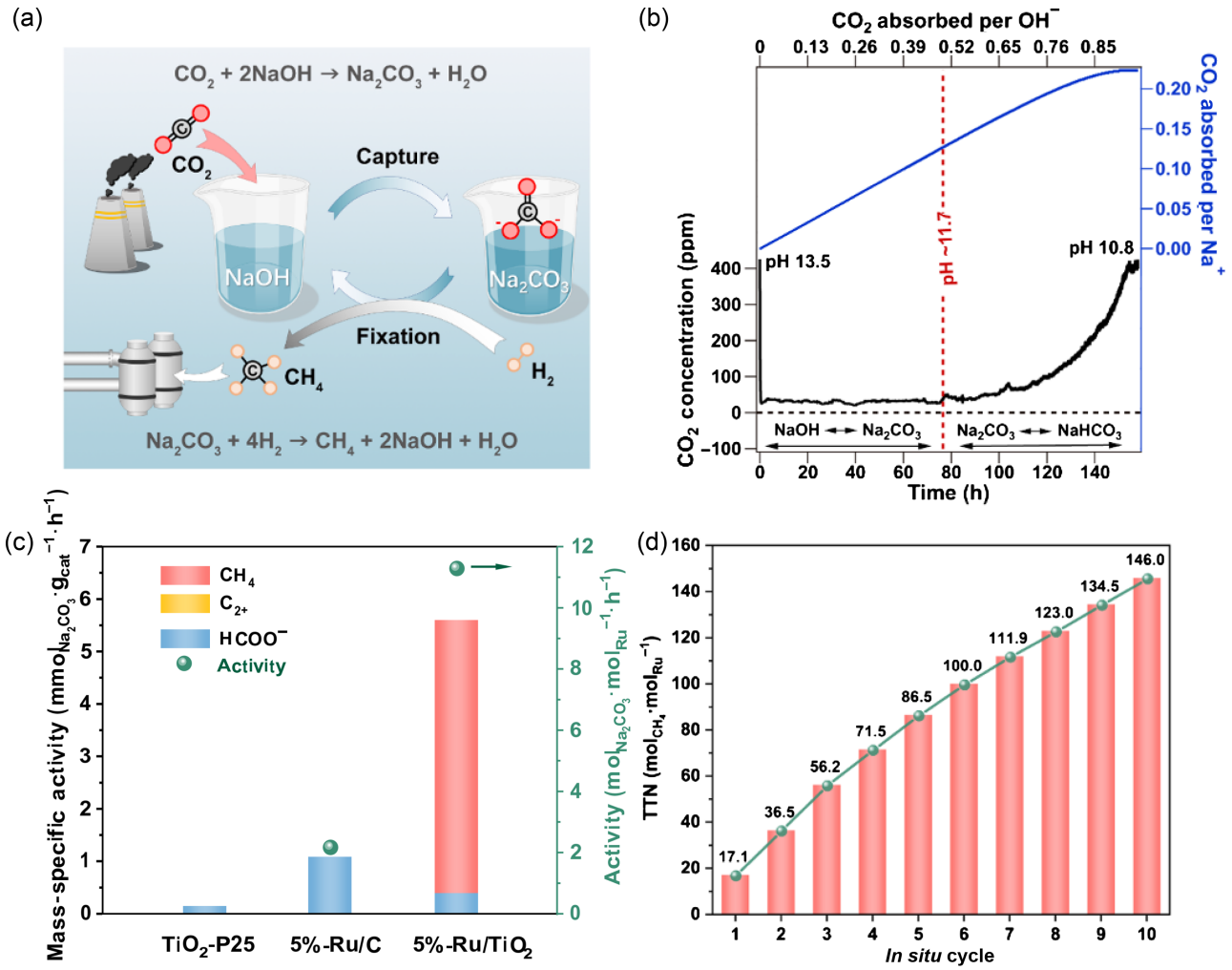

Figure 1 | *CC&M process and catalytic performance of Ru/TiO_2. (a) Schematic diagram of CC&M cycle. Dilute CO_2 in air or industrial emission can be easily captured by alkaline solution like sodium hydroxide solution, and the formed carbonate can be converted by catalysis (with renewable hydrogen) into methane and recycle back the alkaline solution for the next capture and fixation cycle. (b) Laboratory-scale CO_2 air capture test at room temperature using ambient air containing ~400 ppm CO_2 as the feed. (c) Catalytic performance of TiO_2, 5%-Ru/C, and 5%-Ru/TiO_2 catalyst in aqueous-phase Na_2CO_3 hydrogenation (463 K, 3 MPa H_2). (d) Stability of 5%-Ru/TiO_2 catalyst in CC&M cycles (463 K, 3 MPa H_2). TTN, total turnover number.*

catalytic system to convert this CO_2 capture product into valuable chemicals, such as methane. Hydrogenation of aqueous carbonate solution was evaluated on a series of supported metal catalysts at 3 MPa of H_2 and 463 K (Table 1). Negligible activity was observed on the blank TiO_2 support, with a 0.8% conversion of carbonate after 3 h and a trace amount of formate. On Ru/C and Ni/TiO_2 and Rh/TiO_2 (5 wt % metal loading) catalysts, formate was the main product (selectivity >85%), while Ru/CeO_2 produced a mixture of methane, C_{2+} hydrocarbons, and formate (Table 1, entries 2–5). Importantly, carbonate was selectively hydrogenated to methane on Ru nanoparticles supported on TiO_2 (5%-Ru/TiO_2, Table 1, entry 6). A carbonate conversion rate of 11.3 $mol_{Na2CO3} \cdot mol_{Ru}^{-1} \cdot h^{-1}$ was achieved at 463 K in an aqueous solution of sodium carbonate (25 mmol carbonate), with a methane selectivity of 93.0% (Figure 1c). This rate is comparable to those observed at 473 K over Rh and alkali-promoted Ru catalysts in the gas-phase CO_2 hydrogenation reaction.[2,25,26] After optimizing the ratio of H_2 to sodium carbonate in the feed, we demonstrate that carbonate conversion of up to 86.3% can be achieved with the methane selectivity exceeding 99% (Table 1, entry 7; 5 mmol carbonate, 3 MPa H_2, 473 K, 3 h). Sodium formate was the only liquid-phase by-product, along with a trace amount of gas-phase C_{2+} hydrocarbons. CO was not detected (Supporting Information Figure S1). Thus, methane was the sole gas phase product (with a selectivity of 99.9%). As will be discussed later, formate is a reaction intermediate en route to methane. Therefore, the overall

Citation: *CCS Chem.* **2023**, Just Published. DOI: 10.31635/ccschem.023.202303594
Link to VoR: https://doi.org/10.31635/ccschem.023.202303594

Table 1 | *Catalytic Performance of TiO_2 and Supported Catalysts for Hydrogenation of Aqueous Carbonate Solution*

Entry	Catalyst	Conversion (%)	Mass-Specific Activity ($mmol_{Na2CO3}·g_{cat.}^{-1}·h^{-1}$)	Selectivity (%) CH_4	C_{2+}	$HCOO^-$
1	TiO_2-P25[a]	0.8	0.16	—	—	>99.9
2	5%-Ru/C[b]	5.2	1.08	—	—	>99.9
3	5%-Ni/TiO_2	16.8	3.51	11.5	0.1	88.3
4	5%-Rh/TiO_2	15.2	3.17	7.8	—	92.2
5	5%-Ru/CeO_2	9.7	2.02	66.7	4.4	28.9
6	5%-Ru/TiO_2	26.9	5.60	93.0	0.1	6.9
7	5%-Ru/TiO_2[c]	86.3	3.60	99.1	—	0.9

Reaction conditions: 400 mg catalyst, 35 mL H_2O, 25 mmol Na_2CO_3, 3.0 MPa H_2 (10 vol % Ar as the internal standard), 463 K, 3 h.
[a] Commercial catalyst purchased from Evonik Industries AG.
[b] Commercial catalyst purchased from Shanghai Macklin Biochemical Co., Ltd. (Shanghai, China).
[c] 5 mmol Na_2CO_3 was used as the substrate.

reaction converts carbonate to a single product (methane) without accumulating organic carbon species over repeated runs. The Ru/TiO_2 catalyst exhibited excellent stability during 10 consecutive reactivity tests with minimal regeneration between runs (see Supporting Information Stability Evaluation). A cumulative turnover number of 146.0 $mol_{CH4}·mol_{Ru}^{-1}$ was achieved (Figure 1d). The pH of the solution increased from 11.8 to 13.6 after reaction due to the production of 2 units of OH^- upon hydrogenating 1 unit of CO_3^{2-}, suggesting that this reaction can maintain the solution alkalinity when it is coupled with DAC of CO_2.

The ability to simultaneously achieve high carbonate conversion and near exclusive methane selectivity is key to scaling up and intensifying the proposed CC&M process for three reasons: (1) it enables the integration of capture and conversion of CO_2 without the energetically costly temperature swing adsorption in existing DAC strategies; (2) methane spontaneously separates from the aqueous reaction medium, thus avoiding product separation; and (3) the majority of captured CO_2 is converted each cycle with the high conversion of carbonate, enhancing the throughput of the entire process. These considerations are shown to be key to the economic viability of the proposed CC&M process via the technoeconomic analysis presented in the next section. We should stress that no parametric optimization of reactivity has been conducted in this proof-of-concept study, as the focus is on demonstrating an effective strategy for the combined CO_2 DAC and fixation process.

To verify the feasibility of the proposed process, we performed engineering/energy simulations based on a CC&M plant using the concept described above with a capacity of 1 Mt/y CO_2 (Aspen Plus V10, Bedford, Massachusetts, United States; Figure 2a and Supporting Information Figure S2). A state-of-the-art CO_2 capture protocol proposed recently[27] was adapted in our simulations. A heat exchange system was employed to recycle

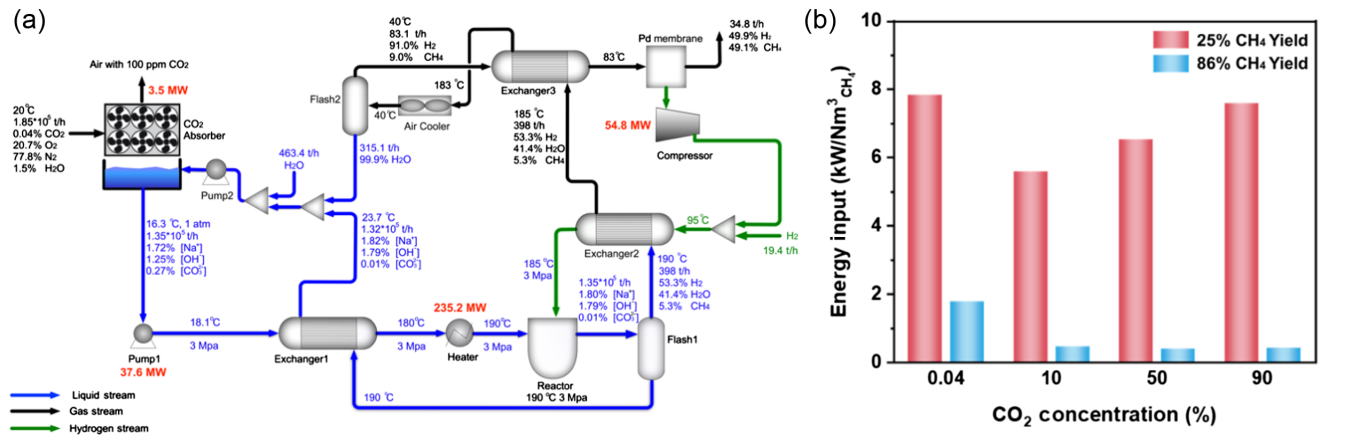

Figure 2 | *Energy/mass analysis of the CC&M process. (a) Flow diagram of CC&M process showing mass and energy balances. 400 ppm CO_2 is used and CH_4 yield is assumed to be 90%. (b) Energy input of the CC&M process at different working conditions. CO_2 of different concentrations (400 ppm, 10%, 50%, 90%) are used as the feed gas, and two different levels of CH_4 yield are considered.*

Citation: *CCS Chem.* **2023**, Just Published. DOI: 10.31635/ccschem.023.202303594
Link to VoR: https://doi.org/10.31635/ccschem.023.202303594

heat from the hot stream vent from the reactor to the cold feed H_2 or sodium carbonate solution and to separate methane from the unreacted H_2 and steam. The simulation results, with full consideration of the carbon and energy balances, clearly demonstrate that the proposed CC&M process is technically feasible, economically viable, and capable of operating continuously. Energy input of CO_2 capture and the hydrogenation (at 463 K) process based on engineering simulations is shown in Supporting Information Table S1 and Figure 2b. When the methane yield is set at 25%, 400 ppm CO_2 (similar to the CO_2 concentration in air) can be captured at a rate of 112 t/h and converted to methane at a rate of 30.2 t/h, and the energy cost for the whole process is 7.8 kWh/(Nm^3_{CH4}) (Supporting Information Table S1, Case 1). When the methane yield increases to 86% (which is achieved under our reaction condition), 400 ppm CO_2 can be captured and converted at a rate of 28.9 t/h for methane production, and the energy cost decreases to 1.9 kWh/(Nm^3_{CH4}) (Supporting Information Table S1, Case 5). The energy cost further drops to 0.5 kWh/(Nm^3_{CH4}) (Supporting Information Table S1, Case 6) when 10% concentrated CO_2 (simulating the case of flue gas) is used as the feed. Considering the energy input of the DAC process using KCRC reported by Heidel et al.[27] (Supporting Information Table S2) is up to 4.8 kWh/(Nm^3_{CO2}), the Na_2CO_3 conversion step is substantially less energy-costly than the $CaCO_3$ calcination step in KCRC. Furthermore, it should be noted that Kenton's proposal is only to separate and enrich CO_2 from the air, while CO_2 is converted to CH_4 in our proposed CC&M process, suggesting that the proposed CC&M strategy has the potential to substantially outperform existing carbon capture technologies. A brief comparison of the proposed CC&M process with other processes reported in the literature is provided in the Supplementary Information.

Matching the CO_2 absorption rate and carbonate conversion rate is another key consideration for continuous operation of the proposed CC&M process. Our process simulations show that the CO_2 absorption rate and methanation reaction rate can be tuned and matched by the energy input of the corresponding units (more details are provided in the Process Engineering Simulation section in the Supporting Information), showing the feasibility of the process. The engineering simulations clearly indicate that mass and energy is balanced in the proposed CC&M process, confirming its viability for potential large-scale application.

We now turn to the fundamentals in the catalytic step of the proposed CC&M strategy. The Ru/TiO_2 catalysts were thoroughly characterized by aberration-corrected scanning transmission electron microscopy (STEM), in-situ X-ray absorption spectroscopy (XAS), X-ray photoemission spectrum (XPS), and DFT calculations, to identify the active sites for the carbonate conversion. The morphology of the fresh and spent catalysts characterized by STEM high-angle annular dark-field (HAADF) imaging are demonstrated in Figure 3. Ru nanoparticles are highly dispersed on the TiO_2 support in the fresh catalyst, with an average diameter of ~1.5 ± 0.4 nm (Figure 3a,b). No notable morphological changes were observed on the spent catalyst (Figure 3c,d). This is corroborated by the lack of diffraction peaks attributable to ruthenium crystallites in X-ray diffraction (XRD) patterns of the fresh and spent catalysts, suggesting the highly dispersed nature of the Ru species without much crystal growth or sintering after the reaction (Figure 3e). In addition, analysis of the high-magnification HAADF images and their fast Fourier transform patterns (Figure 3b,d) indicates that most Ru NPs are situated on the TiO_2 anatase structure with {101} as the preferred facet.

In-situ XAS experiments were conducted at reaction conditions (463 K, 3 MPa H_2, in the presence of aqueous sodium carbonate) to determine the oxidation state and bonding environment of Ru species in the catalyst in the present work. X-ray absorption near-edge structure (XANES) spectroscopy of the Ru/TiO_2 catalyst shows that the fresh sample contains partially oxidized Ru (Figure 3f). As shown in Supporting Information Figures S3–S5 and Table S3, for the fresh 5%-Ru/TiO_2 catalyst, 43.4% is Ru oxide while 56.6% is metallic Ru. The Fourier-transformed k^2-weighted extended X-ray absorption fine structure (EXAFS) provides evidence of the coordination environment of Ru species supported over TiO_2 (Figure 3g). Besides the Ru–Ru scattering at 2.70 Å, a peak at around 1.93 Å can be assigned to Ru-O coordination (Supporting Information Table S4), which agrees well with the XANES obervation. Upon hydrogen pretreatment at 623 K, the Ru in the activated Ru/TiO_2 catalyst is largely reduced to the metallic state, as evidenced by the similar X-ray absorption edges of the activated catalyst to that of the reference Ru foil. Ru K-edge EXAFS results show that the Ru–Ru coodination number ($C.N._{Ru-Ru}$) increases from 4.0 ± 0.8 to 8.1 ± 0.6, and the Ru-O coordination number ($C.N._{Ru-O}$) decreases from 3.0 ± 1.1 to 0.2 ± 0.2 after the hydrogen pretreatment (Figure 3h). This suggests that the Ru particles in the activated catalyst are largely metallic and only a small fraction of Ru is partially oxidized, which is likely located at the interface with the TiO_2 substrate (Supporting Information Figure S6).[28] Indeed, from linear combination fitting (LCF) of XANES, it is clear that metallic Ru becomes the dominant species with the contribution of Ru oxide at around 11.8%. Deconvoluted Ru 3*d* XPS spectrum of the Ru/TiO_2 catalyst after H_2 pretreatment (transferred to the XPS chamber in an inert atomphere) shows the presence of 13% Ru oxide species (Figure 3i), further confirming the presence of partially oxidized interfacial Ru atoms in contact with the TiO_2 support.[29,30]

The oxidation state of Ru species remained unchanged when the catalyst was introduced into the reaction mixture at room temperature (Figure 3f). Upon increasing

Citation: *CCS Chem.* **2023**, Just Published. DOI: 10.31635/ccschem.023.202303594
Link to VoR: https://doi.org/10.31635/ccschem.023.202303594

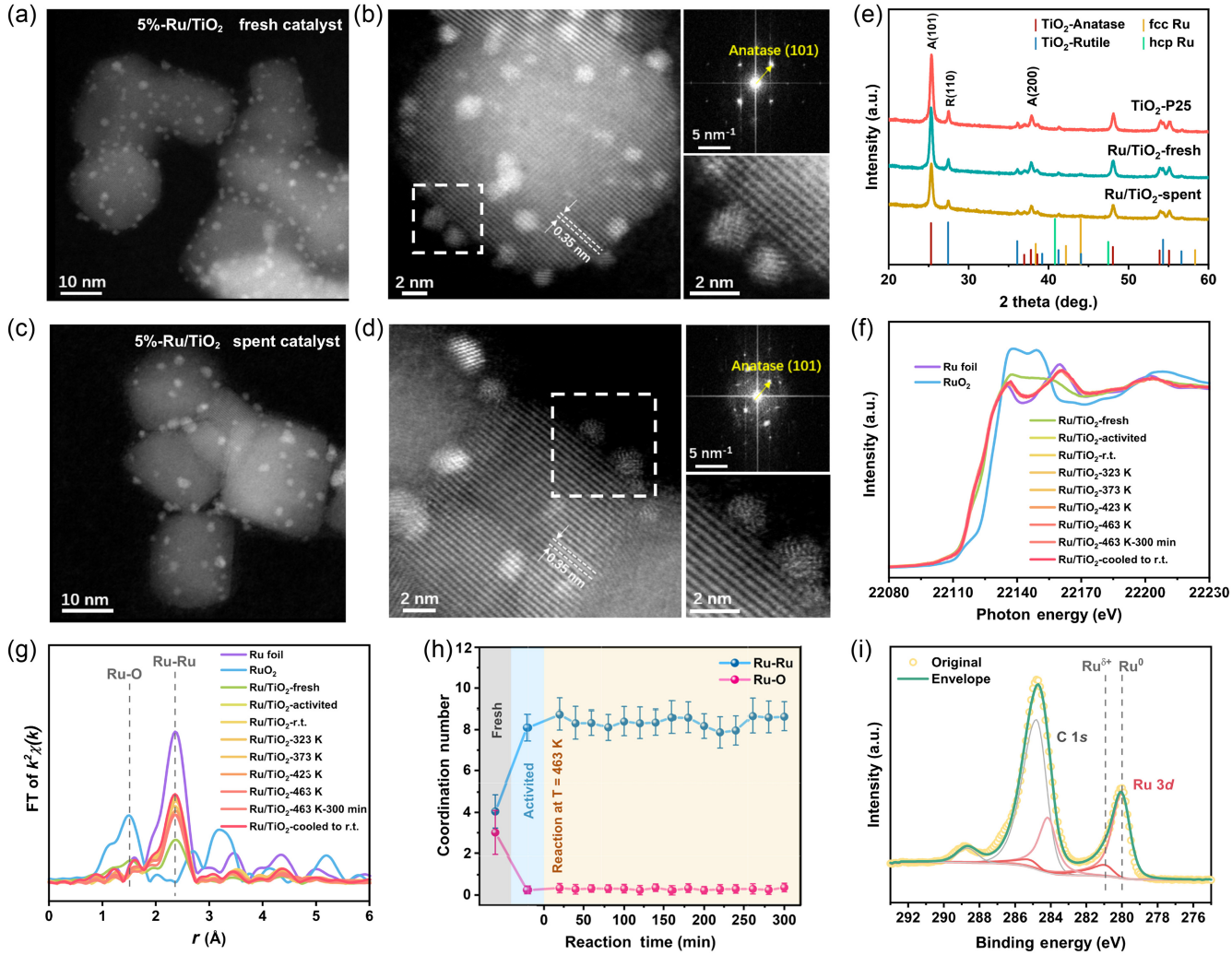

Figure 3 | *Structural characterization of the 5%-Ru/TiO_2 catalyst. (a, b) STEM-HAADF images of 5%-Ru/TiO_2 fresh catalyst. (c, d) STEM-HAADF images of 5%-Ru/TiO_2 spent catalyst. (e) XRD patterns of TiO_2-P25 support, fresh and spent 5%-Ru/TiO_2 catalysts. (f) Ru K-edge XANES spectra of 5%-Ru/TiO_2 catalyst for in-situ XAS measurements during aqueous-phase Na_2CO_3 hydrogenation reaction under high pressure (around 3 MPa) and 463 K. (g) Corresponding Ru K-edge EXAFS fitting results of 5%-Ru/TiO_2 catalyst for in-situ XAS measurements. (h) Ru–Ru and Ru-O coordination numbers as a function of reaction process during in-situ XAS measurements. Error bars represent the fitting error of coordination numbers from EXAFS. (i) Deconvoluted Ru 3d XPS spectrum of the activated Ru/TiO_2 catalyst.*

the reaction temperature to 463 K, the oxidation state of Ru and the $C.N._{Ru-Ru}$ remained largely unchanged (Figures 3f–h), and remained so during reaction for 5 h (Supporting Information Figures S7 and S8), suggesting that the Ru/TiO_2 catalyst is structurally stable under reaction conditions. Consistent with these results, the Ru-O coordination number showed no significant change during the course of the reaction. The structural characterization results and the drastic difference in methane selectivity between the 5%-Ru/TiO_2 and other catalysts (Table 1) hint at the critical role of both interfacial Ru and metallic Ru for the methane production. To further understand the role of Ru/TiO_2 interface in the aqueous carbonate hydrogenation reaction, we studied the catalytic performace of a series of Ru/TiO_2 catalysts with different Ru loadings and different interfacial Ru contents (see Supporting Information Figures S9 and S10 and associated discussion in the Supporting Information for detail). The results show that formate can easily form at the interfacial $Ru^{\delta+}$ sites (Supporting Information Figure S6) while adjacent metallic Ru^0 sites are necessary for the production of methane.

Implicit solvent DFT calculations were performed to understand the carbonate hydrogenation mechanism over the Ru/TiO_2 catalyst, which was modeled by Ru_{10}/TiO_2(101) based on the STEM result (Figure 3b). We used a genetic algorithm to identify the global minimum structure of the TiO_2(101)-supported Ru_{10} cluster with a

Citation: *CCS Chem.* **2023**, Just Published. DOI: 10.31635/ccschem.023.202303594
Link to VoR: https://doi.org/10.31635/ccschem.023.202303594

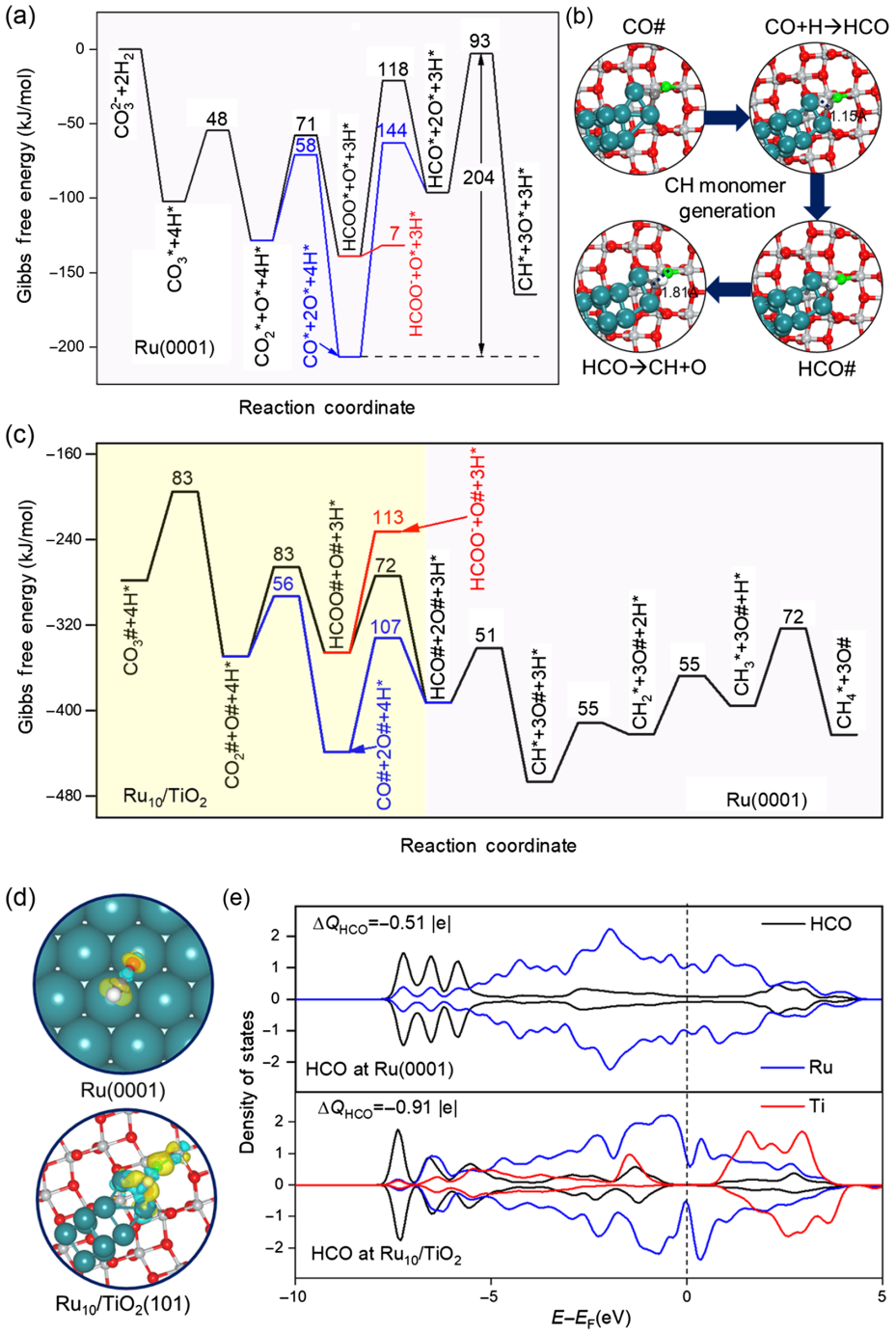

Figure 4 | *DFT studies of the CO_3^{2-} hydrogenation mechanism. (a) Potential energy surface for carbonate hydrogenation toward formate over the Ru(0001) surface. * indicates the empty site on Ru. All the elementary activation barriers are indicated in kJ/mol. The infinitely separated adsorbed intermediates were considered for the energetics calculations. (b) Configurations for HCO intermediate adsorption and dissociation at the interface of the Ru_{10}/TiO_2 surface. The cyan, light gray, red/green, gray, and white spheres are Ru, Ti, O, C, and H atoms, respectively. The bond distances between two fragments at the transition state configuration for HCO formation and dissociation at the interface of the Ru/TiO_2 catalyst are given in Å. (c) Potential energy surface for carbonate hydrogenation toward CH monomers at the interface of the Ru_{10}/TiO_2 surface and subsequent CH methanation on the Ru(0001) surface. # indicates the empty site at the interface of Ru_{10}/TiO_2 surface. (d) The differential charge density of HCO intermediate adsorption on Ru(0001) and Ru_{10}/TiO_2 surfaces with an isosurface value of 0.007 e/Å^3. Yellow and cyan colors represent charge depletion and accumulation, respectively. (e) Partial density of states (PDOS) for HCO intermediate adsorption on Ru(0001) and Ru_{10}/TiO_2 surfaces. The total charge transfer from the surface to the HCO intermediate is indicated by ΔQ_{HCO}. The dashed line shows the Fermi level.*

Citation: *CCS Chem.* **2023**, Just Published. DOI: 10.31635/ccschem.023.202303594
Link to VoR: https://doi.org/10.31635/ccschem.023.202303594

diameter of ~0.89 nm, which is close to the experimental value. For reference, we first investigated Ru(0001) and the calculated Gibbs free energy surface for carbonate hydrogenation, showing that direct CO_2 dissociation into CO is slightly more preferable than hydrogen-assisted CO_2 reduction to formate by 13 kJ/mol. However, further hydrogen-assisted CO to form a highly endothermic HCO intermediate and subsequently to the CH monomer necessary for methane formation requires an overall barrier as high as 204 kJ/mol, which is unfeasible under the reaction conditions considered (Figure 4a). However, the formate produced from the CO_2 reduction binds weakly and tends to desorb from the surface rather than dissociate into the CH intermediate for further hydrogenation to form methane (Figure 4a, Supporting Information Table S7 and Figures S11 and S12). As a result, formate is the main product for carbonate hydrogenation over metallic Ru catalysts, which is corroborated by our experimental measurements (Table 1).

Compared with metallic Ru, we found that direct CO_2 dissociation into CO at Ru_{10}/TiO_2 is also more preferable than CO_2 reduction to formate by 27 kJ/mol (Figure 4b,c and Supporting Information Tables S8 and S9). Different from metallic Ru, hydrogen-assisted CO activation to form HCO and subsequent CH monomers at Ru_{10}/TiO_2 (Supporting Information Figure S13) has a much lower overall barrier of 107 kJ/mol. The favorable kinetics are mainly driven by a highly exothermic reaction energy for CO activation (Figure 4c and Supporting Information Figure S14) due to the stronger adsorption of HCO (–299 vs –203 kJ/mol, Supporting Information Figure S14) and/or O (–322 vs –222 kJ/mol, Supporting Information Figure S14), which can be rationalized by significant orbital hybridization and charge transfer between HCO/O and Ti atoms in Ru_{10}/TiO_2 (Figure 4d,e and Supporting Information Figure S15). Once favorable HCO was formed, subsequent C–O bond breaking and formation of CH monomer and methane over Ru metallic sites were facile (Figure 4c). As a result, the major product of carbonate hydrogenation is methane in the presence of the Ru_{10}/TiO_2 interface. We note that although formate could form on metallic Ru sites, it readsorbs at the Ru_{10}/TiO_2 interface to dissociate into HCO to eventually form methane, as indicated above (Figure 4c), thus improving methane selectivity. Our calculations are corroborated by the experimental measurement that formate can be hydrogenated toward methane at the interface of Ru/TiO_2 catalyst (Supporting Information Figure S16 and Table S10). Therefore, the interfacial sites over Ru/TiO_2 are essential for carbonate hydrogenation toward methane with high selectivity.

The role of formate as a reaction intermediate toward methane formation is also supported by the time evolution of the product distribution in the aqueous carbonate hydrogenation reaction. The yield of formate reached up to 4.5% after the first 0.25 h of reaction and fell to 0.9% after 10 h (Supporting Information Figure S17). This is a hallmark of a reactive intermediate in a sequential reaction network.[31] As a reactive intermediate, formate does not accumulate in the solution and leads to carbon loss in the proposed CC&M scheme.

Conclusion

In summary, we report an integrated aqueous phase CC&M process. An overall selectivity of 99.9% for methane production in gas-phase products is achieved on the 5%-Ru/TiO_2 catalyst, which enables facile separation of the product from the reaction system. Engineering simulations demonstrate that the CC&M process is energetically viable, showing promise for potential large-scale applications.

Supporting Information

Supporting Information is available and includes experimental details, supporting discussions, Figures S1–S18, and Tables S1–S18.

Conflict of Interest

There is no conflict of interest to declare.

Acknowledgments

This work received financial support from the Natural Science Foundation of China (grant nos. 21725301, 21932002, 21821004, 91645115, 51872008, 22172183, 22172150, and 22222306), the National Key R&D Program of China (grant nos. 2017YFB060220 and 2021YFA1502804), the Beijing Outstanding Young Scientists Projects (grant nos. BJJWZYJH01201910005018 and BJJWZYJH01201914430039), the Strategic Priority Research Program of the Chinese Academy of Science (grant no. XDB0450102), the K.C. Wong Education Foundation (grant no. GJTD-2020-15), and the Innovation Program for Quantum Science and Technology (grant no. 2021ZD0303302). The XAS spectroscopy studies were conducted at the Shanghai Synchrotron Radiation Facility and the Beijing Synchrotron Radiation Facility. D.M. acknowledges support from the Tencent Foundation through the XPLORER PRIZE. B.M.W. thanks the Netherlands Center for Multiscale Catalytic Energy Conversion, an NWO Gravitation Program funded by the Ministry of Education, Culture, and Science of the government of the Netherlands, for funding. J.L. thanks the high-performance computational resources provided by the University of Science and Technology of China (http://scc.ustc.edu.cn) and the Hefei Advanced Computing Center.

Citation: *CCS Chem.* **2023**, Just Published. DOI: 10.31635/ccschem.023.202303594
Link to VoR: https://doi.org/10.31635/ccschem.023.202303594

References

1. Letcher, T. M. Chapter 1—Introduction with a Focus on Atmospheric Carbon Dioxide and Climate Change. In *Future Energy*, 2nd ed.;Letcher, T. M., Ed.; Elsevier: Boston, MA, **2014**.
2. Vogt, C.; Monai, M.; Kramer, G. J.; Weckhuysen, B. M. The Renaissance of the Sabatier Reaction and Its Applications on Earth and in Space. *Nat. Catal.* **2019**, *2*, 188–197.
3. Masson-Delmotte, V.; Zhai, P.; Pörtner, H.-O.; Roberts, D.; Skea, J.; Shukla, P. R.; Pirani, A.; Moufouma-Okia, W.; Péan, C.; Pidcock, R.; Connors, S.; Matthews, J. B. R.; Chen, Y.; Zhou, X.; Gomis, M. I.; Lonnoy, E.; Maycock, T.; Tignor, M.; Waterfield, T. *Global Warming of 1.5°C. An IPCC Special Report on the Impacts of Global Warming of 1.5°C Above Pre-Industrial Levels and Related Global Greenhouse Gas Emission Pathways, in the Context of Strengthening the Global Response to the Threat of Climate Change, Sustainable Development, and Efforts to Eradicate Poverty*; Intergovernmental Panel on Climate Change: Geneva, **2018**.
4. Kim, E. J.; Siegelman, R. L.; Jiang, H. Z. H.; Forse, A. C.; Lee, J. H.; Martell, J. D.; Milner, P. J.; Falkowski, J. M.; Neaton, J. B.; Reimer, J. A.; Weston, S. C.; Long, J. R. Cooperative Carbon Capture and Steam Regeneration with Tetraamine-Appended Metal-Organic Frameworks. *Science* **2020**, *369*, 392–396.
5. Aresta, M.; Dibenedetto, A.; Angelini, A. Catalysis for the Valorization of Exhaust Carbon: From CO_2 to Chemicals, Materials, and Fuels. Technological Use of CO_2. *Chem. Rev.* **2014**, *114*, 1709–1742.
6. Didas, S. A.; Choi, S.; Chaikittisilp, W.; Jones, C. W. Amine-Oxide Hybrid Materials for CO_2 Capture from Ambient Air. *Acc. Chem. Res.* **2015**, *48*, 2680–2687.
7. Socolow, R.; Desmond, M.; Aines, R.; Blackstock, J.; Bolland, O.; Kaarsberg, T.; Lewis, N.; Mazzotti, M.; Pfeffer, A.; Sawyer, K. *Direct Air Capture of CO_2 with Chemicals: A Technology Assessment for the APS Panel on Public Affairs*; American Physical Society: College Park, MD, **2011**.
8. Nikulshina, V.; Ayesa, N.; Galvez, M.; Steinfeld, A. Feasibility of Na-Based Thermochemical Cycles for the Capture of CO_2 from Air—Thermodynamic and Thermogravimetric Analyses. *Chem. Eng. J.* **2008**, *140*, 62–70.
9. Keith, D. W. Why Capture CO_2 from the Atmosphere? *Science* **2009**, *325*, 1654–1655.
10. Singh, S. P.; Hao, P.; Liu, X.; Wei, C.; Xu, W. Q.; Wei, N.; Li, X.; Lu, H.; Ku, A. Y. Large-Scale Affordable CO_2 Capture is Possible by 2030. *Joule* **2019**, *3*, 2154–2164.
11. Kattel, S.; Ramirez, P. J.; Chen, J. G.; Rodriguez, J. A.; Liu, P. Active Sites for CO_2 Hydrogenation to Methanol on Cu/ZnO Catalysts. *Science* **2017**, *355*, 1296–1299.
12. Rao, H.; Schmidt, L. C.; Bonin, J.; Robert, M. Visible-Light-Driven Methane Formation from CO_2 with a Molecular Iron Catalyst. *Nature* **2017**, *548*, 74–77.
13. Liu, M.; Pang, Y.; Zhang, B.; De Luna, P.; Voznyy, O.; Xu, J.; Zheng, X.; Dinh, C. T.; Fan, F.; Cao, C.; de Arquer, F. P.; Safaei, T. S.; Mepham, A.; Klinkova, A.; Kumacheva, E.; Filleter, T.; Sinton, D.; Kelley, S. O.; Sargent, E. H. Enhanced Electrocatalytic CO_2 Reduction via Field-Induced Reagent Concentration. *Nature* **2016**, *537*, 382–386.
14. Li, F.; Thevenon, A.; Rosas-Hernandez, A.; Wang, Z.; Li, Y.; Gabardo, C. M.; Ozden, A.; Dinh, C. T.; Li, J.; Wang, Y.; Edwards, J. P.; Xu, Y.; McCallum, C.; Tao, L.; Liang, Z. Q.; Luo, M.; Wang, X.; Li, H.; O'Brien, C. P.; Tan, C. S.; Nam, D. H.; Quintero-Bermudez, R.; Zhuang, T. T.; Li, Y. C.; Han, Z.; Britt, R. D.; Sinton, D.; Agapie, T.; Peters, J. C.; Sargent, E. H. Molecular Tuning of CO_2-to-Ethylene Conversion. *Nature* **2020**, *577*, 509–513.
15. Mariano, R. G.; McKelvey, K.; White, H. S.; Kanan, M. W. Selective Increase in CO_2 Electroreduction Activity at Grain-Boundary Surface Terminations. *Science* **2017**, *358*, 1187–1191.
16. Buelens, L. C.; Galvita, V. V.; Poelman, H.; Detavernier, C.; Marin, G. B. Super-Dry Reforming of Methane Intensifies CO_2 Utilization via Le Chatelier's Principle. *Science* **2016**, *354*, 449–452.
17. Gao, D.; Aran-Ais, R. M.; Jeon, H. S.; Roldan Cuenya, B. Rational Catalyst and Electrolyte Design for CO_2 Electroreduction Towards Multicarbon Products. *Nat. Catal.* **2019**, *2*, 198–210.
18. Porosoff, M. D.; Yan, B. H.; Chen, J. G. G. Catalytic Reduction of CO_2 by H_2 for Synthesis of CO, Methanol and Hydrocarbons: Challenges and Opportunities. *Energy Environ. Sci.* **2016**, *9*, 62–73.
19. Kar, S.; Goeppert, A.; Galvan, V.; Chowdhury, R.; Olah, J.; Prakash, G. K. S. A Carbon-Neutral CO_2 Capture, Conversion, and Utilization Cycle with Low-Temperature Regeneration of Sodium Hydroxide. *J. Am. Chem. Soc.* **2018**, *140*, 16873–16876.
20. Kar, S.; Sen, R.; Goeppert, A.; Prakash, G. K. S. Integrative CO_2 Capture and Hydrogenation to Methanol with Reusable Catalyst and Amine: Toward a Carbon Neutral Methanol Economy. *J. Am. Chem. Soc.* **2018**, *140*, 1580–1583.
21. Sen, R.; Goeppert, A.; Kar, S.; Prakash, G. K. S. Hydroxide Based Integrated CO_2 Capture from Air and Conversion to Methanol. *J. Am. Chem. Soc.* **2020**, *142*, 4544–4549.
22. Crabtree, R. H. Alternate Strategies for Solar Fuels from Carbon Dioxide. *ACS Energy Lett.* **2020**, *5*, 2505–2507.
23. Wang, L.; Chen, W.; Zhang, D.; Du, Y.; Amal, R.; Qiao, S.; Bf, J. W.; Yin, Z. Surface Strategies for Catalytic CO_2 Reduction: From Two-Dimensional Materials to Nanoclusters to Single Atoms. *Chem. Soc. Rev.* **2019**, *48*, 5310–5349.
24. Teramura, K.; Hori, K.; Terao, Y.; Huang, Z.; Iguchi, S.; Wang, Z.; Asakura, H.; Hosokawa, S.; Tanaka, T. Which Is an Intermediate Species for Photocatalytic Conversion of CO_2 by H_2O as the Electron Donor: CO_2 Molecule, Carbonic Acid, Bicarbonate, or Carbonate Ions? *J. Phys. Chem. C* **2017**, *121*, 8711–8721.
25. Matsubu, J. C.; Yang, V. N.; Christopher, P. Isolated Metal Active Site Concentration and Stability Control Catalytic CO_2 Reduction Selectivity. *J. Am. Chem. Soc.* **2015**, *137*, 3076–3084.

Citation: *CCS Chem.* **2023**, Just Published. DOI: 10.31635/ccschem.023.202303594
Link to VoR: https://doi.org/10.31635/ccschem.023.202303594

26. Petala, A.; Panagiotopoulou, P. Methanation of CO_2 over Alkali-Promoted Ru/TiO_2 Catalysts: I. Effect of Alkali Additives on Catalytic Activity and Selectivity. *Appl. Catal. B* **2018**, *224*, 919–927.
27. Keith, D. W.; Holmes, G.; St. Angelo, D.; Heidel, K. A Process for Capturing CO_2 from the Atmosphere. *Joule* **2018**, *2*, 1573–1594.
28. Zhang, Y.; Yang, X.; Yang, X.; Duan, H.; Qi, H.; Su, Y.; Liang, B.; Tao, H.; Liu, B.; Chen, D.; Su, X.; Huang, Y.; Zhang, T. Tuning Reactivity of Fischer-Tropsch Synthesis by Regulating TiO_x Overlayer over Ru/TiO_2 Nanocatalysts. *Nat. Commun.* **2020**, *11*, 3185.
29. Di, L.; Wu, G.; Dai, W.; Guan, N.; Li, L. Ru/TiO_2 for the Preferential Oxidation of CO in H_2-Rich Stream: Effects of Catalyst Pre-Treatments and Reconstruction of Ru Sites. *Fuel* **2015**, *143*, 318–326.
30. Moulder, J. F.; Stickle, W. F.; Sobol, P. E.; Bomben, K. D. *Handbook of X-Ray Photoelectron Spectroscopy. A Reference Book of Standard Spectra for Identification and Interpretation of XPS Data*, 2nd ed.; Perkin Elmer Corporation: Eden Prairie, MN, **1992**.
31. Houston, P. L. *Chemical Kinetics and Reaction Dynamics*; Dover Publications: New York, **2006**.

Citation: *CCS Chem.* **2023**, Just Published. DOI: 10.31635/ccschem.023.202303594
Link to VoR: https://doi.org/10.31635/ccschem.023.202303594